−1 V bias 67 GHz bandwidth Si-contacted germanium waveguide p-i-n photodetector for optical links at 56 Gbps and beyond

H. Chen,[1,2,*] P. Verheyen,[1] P. De Heyn,[1] G. Lepage,[1] J. De Coster,[1] S. Balakrishnan,[1] P. Absil,[1] W. Yao,[3] L. Shen,[3] G. Roelkens,[2] and J. Van Campenhout[1]

[1]imec, Kapeldreef 75, Leuven B-3001, Belgium
[2]Photonics Research Group, Department of Information Technology, Ghent University—imec, B-9000 Ghent, Belgium
[3]Photonic Integration Group, Eindhoven University of Technology, 5600 MB Eindhoven, Netherlands
*hongtao.chen@imec.be

Abstract: We demonstrate a 67 GHz bandwidth silicon-contacted germanium waveguide p-i-n photodetector operating at −1 V with 6.8 fF capacitance. The dark current is below 4 nA. The responsivity is 0.74 A/W at 1550 nm and 0.93 A/W at 1310 nm wavelength. 56 Gbps on-off-keying data reception is demonstrated with clear open eye diagrams in both the C-band and O-band.

References and links

1. T. Yin, R. Cohen, M. M. Morse, G. Sarid, Y. Chetrit, D. Rubin, and M. J. Paniccia, "31 GHz Ge n-i-p waveguide photodetectors on Silicon-on-Insulator substrate," Opt. Express **15**(21), 13965–13971 (2007).
2. L. Vivien, J. Osmond, J. M. Fédéli, D. Marris-Morini, P. Crozat, J. F. Damlencourt, E. Cassan, Y. Lecunff, and S. Laval, "42 GHz p.i.n Germanium photodetector integrated in a silicon-on-insulator waveguide," Opt. Express **17**(8), 6252–6257 (2009).
3. D. Feng, S. Liao, P. Dong, N.-N. Feng, H. Liang, D. Zheng, C.-C. Kung, J. Fong, R. Shafiiha, J. Cunningham, A. V. Krishnamoorthy, and M. Asghari, "High-speed Ge photodetector monolithically integrated with large cross-section silicon-on-insulator waveguide," Appl. Phys. Lett. **95**(26), 261105 (2009).
4. S. Liao, N.-N. Feng, D. Feng, P. Dong, R. Shafiiha, C.-C. Kung, H. Liang, W. Qian, Y. Liu, J. Fong, J. E. Cunningham, Y. Luo, and M. Asghari, "36 GHz submicron silicon waveguide germanium photodetector," Opt. Express **19**(11), 10967–10972 (2011).
5. C. T. DeRose, D. C. Trotter, W. A. Zortman, A. L. Starbuck, M. Fisher, M. R. Watts, and P. S. Davids, "Ultra compact 45 GHz CMOS compatible Germanium waveguide photodiode with low dark current," Opt. Express **19**(25), 24897–24904 (2011).
6. L. Vivien, A. Polzer, D. Marris-Morini, J. Osmond, J. M. Hartmann, P. Crozat, E. Cassan, C. Kopp, H. Zimmermann, and J. M. Fédéli, "Zero-bias 40Gbit/s germanium waveguide photodetector on silicon," Opt. Express **20**(2), 1096–1101 (2012).
7. G. Li, Y. Luo, X. Zheng, G. Masini, A. Mekis, S. Sahni, H. Thacker, J. Yao, I. Shubin, K. Raj, J. E. Cunningham, and A. V. Krishnamoorthy, "Improving CMOS-compatible Germanium photodetectors," Opt. Express **20**(24), 26345–26350 (2012).
8. A. Novack, M. Gould, Y. Yang, Z. Xuan, M. Streshinsky, Y. Liu, G. Capellini, A. E.-J. Lim, G.-Q. Lo, T. Baehr-Jones, and M. Hochberg, "Germanium photodetector with 60 GHz bandwidth using inductive gain peaking," Opt. Express **21**(23), 28387–28393 (2013).
9. T.-Y. Liow, N. Duan, A. E.-J. Lim, X. Tu, M. Yu, and G.-Q. Lo, "Waveguide Ge/Si avalanche photodetector with a unique low-height-profile device structure," in *Opt. Fiber Commun. Conf.*, (2014), paper M2G.6.
10. Y. Zhang, S. Yang, Y. Yang, M. Gould, N. Ophir, A. E.-J. Lim, G.-Q. Lo, P. Magill, K. Bergman, T. Baehr-Jones, and M. Hochberg, "A high-responsivity photodetector absent metal-germanium direct contact," Opt. Express **22**(9), 11367–11375 (2014).
11. H. Chen, P. Verheyen, P. De Heyn, G. Lepage, J. De Coster, P. Absil, G. Roelkens, and J. Van Campenhout, "High responsivity low-voltage 28Gb/s Ge p-i-n photodetector with silicon contacts," J. Lightwave Technol. **33**(4), 820–824 (2015).
12. R. Going, T. J. Seok, J. Loo, K. Hsu, and M. C. Wu, "Germanium wrap-around photodetectors on Silicon photonics," Opt. Express **23**(9), 11975–11984 (2015).

13. S. Lischke, D. Knoll, C. Mai, L. Zimmermann, A. Peczek, M. Kroh, A. Trusch, E. Krune, K. Voigt, and A. Mai, "High bandwidth, high responsivity waveguide-coupled germanium p-i-n photodiode," Opt. Express **23**(21), 27213–27220 (2015).
14. M. Pantouvaki, P. Verheyen, G. Lepage, J. De Coster, H. Yu, P. De Heyn, P. Absil, and J. Van Campenhout, "20Gb/s silicon ring modulator co-integrated with a Ge monitor photodetector," in *ECOC Conference* (2013), paper We.3.B.2.
15. P. De Heyn, J. De Coster, P. Verheyen, G. Lepage, M. Pantouvaki, P. Absil, W. Bogaerts, J. Van Campenhout, and D. Van Thourhout, "Fabrication-tolerant four-channel wavelength-division-multiplexing filter based on collectively tuned Si microrings," J. Lightwave Technol. **31**(16), 2785–2792 (2013).
16. P. Verheyen, M. Pantouvaki, J. Van Campenhout, P. Absil, H. Chen, P. De Heyn, G. Lepage, J. De Coster, P. Dumon, A. Masood, D. Van Thourhout, R. Baets, and W. Bogaerts, "Highly uniform 25 Gb/s Si photonics platform for high-density, low-power WDM optical interconnects," in *Integr. Photon. Res., Silicon Nanophoton. Conf.* (2014), paper IW3A.4.
17. J. Liu, X. Sun, D. Pan, X. Wang, L. C. Kimerling, T. L. Koch, and J. Michel, "Tensile-strained, n-type Ge as a gain medium for monolithic laser integration on Si," Opt. Express **15**(18), 11272–11277 (2007).

1. Introduction

A germanium waveguide p-i-n photodetector (WPD) is a critical building block in silicon photonics optical interconnects and has been studied extensively [1–13]. Optical receivers based on high opto-electrical bandwidth, high responsivity and low dark current germanium photodetectors substantially enhance the performance of Si-based optical interconnects. Conventional germanium WPDs require doping in germanium as well as a metal contact on germanium to form the p-i-n junction. Light absorption from the metal contacts on germanium is responsible for a substantial responsivity loss in these devices. In addition, the process to form a metal contact to germanium is less well developed in standard CMOS foundries. In [10], a germanium WPD that does not require doping or contacting of germanium (named Si-LPIN GePD hereafter) was demonstrated showing a very high responsivity of 1.14 A/W at 1550 nm wavelength at −4 V bias. The 3-dB opto-electrical bandwidth was 20 GHz. The high bias voltage of −4 V is however not CMOS compatible. We demonstrated such a Si-LPIN GePD operating at −1 V showing high responsivity over 1 A/W across the whole C-band and a very low dark current of 3 nA [11]. However, the opto-electrical 3-dB bandwidth of the device was transit-time limited to 20 GHz at 1550 nm wavelength.

In this paper, by adopting a 160 nm thin germanium layer to reduce the transit time, the opto-electrical 3-dB bandwidth at −1 V is enhanced to 67 GHz and 44 GHz at 1550 nm and 1310 nm, respectively. The junction capacitance is 6.8 fF at −1 V. Light coupling from the silicon-on-insulator (SOI) waveguide to the germanium waveguide is optimized by adding a poly-Si taper on top of the fully etched Si taper. The measured responsivity at −1 V is 0.74 A/W and 0.93 A/W at 1550 nm and 1310 nm respectively. The dark current is as low as 4 nA at −1 V. These device properties make it an attractive candidate for Si photonics optical interconnects. 56 Gbps on-off keying data reception is demonstrated with clear open eye diagrams at both 1550 nm and 1310 nm wavelength. The opto-electrical 3-dB bandwidth beyond 67 GHz at higher reverse bias enables even 100 Gbps on-off keying optical receivers.

2. Device design and fabrication

The Si-LPIN GePDs were fabricated in imec's fully integrated Si Photonics Platform along with Si modulators [14] and various passive devices [15]. They go through a process flow described in [16]. Light is coupled from a 220 nm thick single-mode Si waveguide (450nm wide) to the germanium-on-SOI waveguide using a Si waveguide taper together with a 120 nm thick poly-Si taper, as shown in Fig. 1(a). The germanium layer dimensions and doping configuration in the Si-LPIN GePD are shown in Fig. 1(b). The doping distribution in the Si-LPIN GePD is shown in Fig. 2(a), simulated using *Sentaurus* Process.
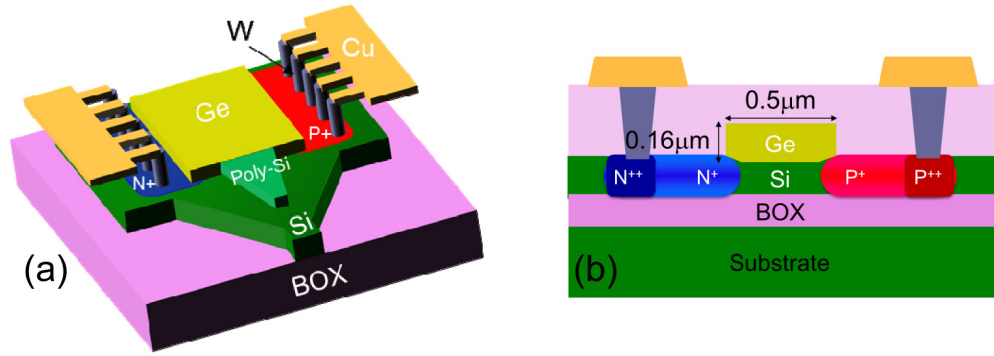
Fig. 1. (a) 3-D schematic of the Si-LPIN GePD. (b) Cross-section schematic of the Si-LPIN GePD with a 0.16 μm thick and 0.5 μm wide germanium layer.
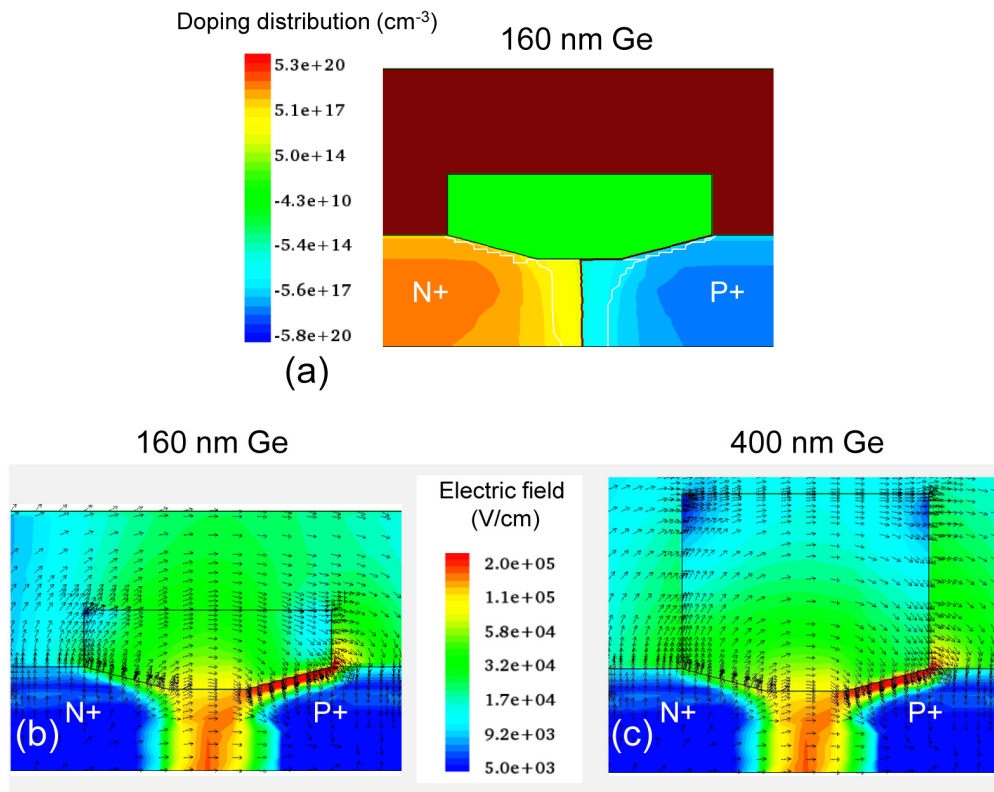
Fig. 2. (a) Simulated doping distribution in the Si-LPIN GePD using *Sentaurus* Process. (b) Simulated electric field distribution in the Si-LPIN GePD reported in this paper at −1 V using *Sentaurus* Device. (c) Simulated electric field distribution at −1 V for a Si-LPIN GePD with a 400 nm thick germanium layer using *Sentaurus* Device. The only difference between the 2 Si-LPIN GePD devices is the germanium layer thickness. The electric field direction is annotated in the graph.

The electric field distribution at −1 V obtained by numerically solving the Poisson's equation using *Sentaurus* Device is shown in Fig. 2(b). In the germanium region, the electric field is stronger than 10^4 V/cm at −1 V, strong enough for photo-generated carriers to drift at their saturation velocity. In [11], a 400 nm thick germanium layer was used in the Si-LPIN GePD, whose opto-electrical bandwidth was limited by the long transit time of the photo-

carriers generated in the top part of the germanium, suffering from low drift velocity as well as long drift distance. The electric field distribution at −1 V of this device is shown in Fig. 2(c) for reference. It is expected that, in the current device, this bandwidth limitation will be eliminated by using a 160 nm thin germanium layer. Therefore, a much higher opto-electrical bandwidth can be expected.

3. Device characteristics

3.1 Static measurements

A typical static current-voltage characteristic of a 14.2 μm long and 0.5 μm wide Si-LPIN GePD is shown in Fig. 3(a). The device exhibits a dark current as low as 2.5 nA and 3.5 nA at −1 V and −2 V. The light current was measured in the C-band at 1550 nm wavelength and in the O-band at 1310 nm wavelength under a received optical power of −5.8 dBm and −2.5 dBm, respectively. The received optical power is the optical power reaching the photodiode, with the fiber grating coupler insertion loss calibrated out using a reference straight waveguide beside the photodetector. The light current is almost constant from 0 V to −2 V owing to the strong built-in electric field that is capable of sweeping out the majority of the photo-generated carriers within their lifetime. The measured responsivity at −1 V is 0.72 A/W and 0.98 A/W at 1550 nm and 1310 nm, respectively.

Wafer-scale dark current data of the Si-LPIN GePD are shown in Fig. 3(b). The mean dark current value is 2.4 nA and 3.6 nA, with a standard deviation of 0.4 nA and 0.8 nA, at −1 V and −2 V, respectively. In Fig. 3(c) and Fig. 3(d), contour plots of the wafer-scale responsivity data of the Si-LPIN GePD at −1 V at 1550 nm and 1310 nm are shown. The mean responsivity value is 0.74 A/W and 0.93 A/W respectively, with a standard deviation of 0.05 A/W.

The wavelength dependence of the responsivity in the C-band and O-band at −1.2 V bias are shown in Fig. 4(a) and Fig. 4(b), respectively. Only responsivity data in a 40 nm optical bandwidth are shown, limited by the optical bandwidth of the fiber-to-chip grating coupler used to interface to the photodetector. The device has a higher responsivity in the O-band than in the C-band, due to the relatively short device length (14.2 μm) and the higher modal absorption coefficient in the O-band. The higher modal absorption coefficient in the O-band further results from both the higher modal confinement factor in the germanium layer and the stronger material absorption coefficient in the germanium layer in the O-band. The drop in responsivity in the C-band is mainly due to the decrease of the germanium absorption coefficient at longer wavelength, as will be discussed later in section 4. It can be improved by increasing the length of the device (i.e. the germanium layer).
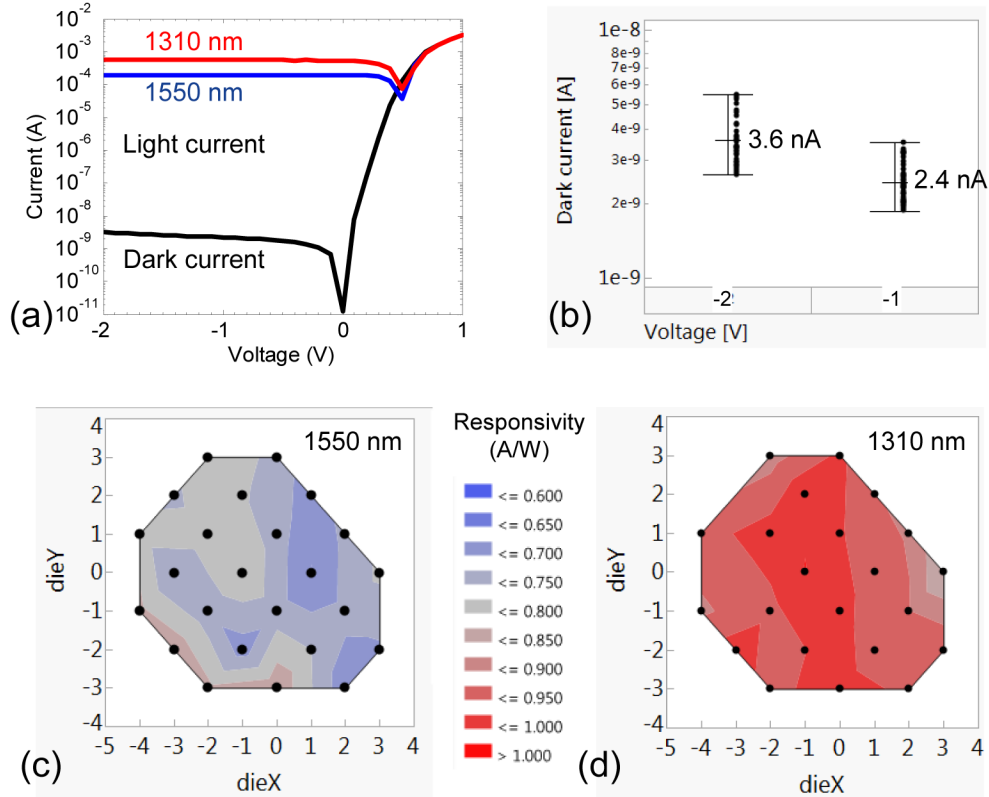
Fig. 3. (a) A typical I-V characteristic of a 14.2 μm long and 0.5 μm wide Si-LPIN GePD. (b) Variability plot of the wafer-scale dark current data of the Si-LPIN GePD at −1 V and −2 V. Contour plot of the wafer-scale responsivity data of the Si-LPIN GePD at (c) 1550 nm and (d) 1310 nm at −1 V.
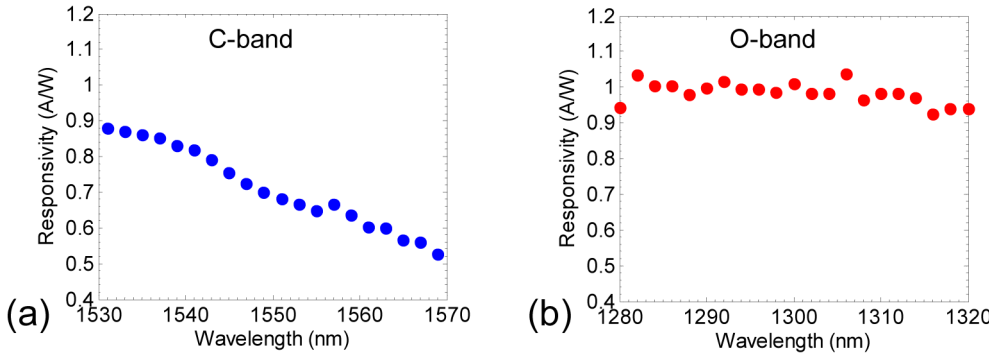
Fig. 4. Responsivity as a function of wavelength of the Si-LPIN GePD in (a) the C-band and (b) the O-band at −1.2 V bias.

3.2 Small-signal measurements

Small-signal radio-frequency (RF) measurements were carried out at wafer scale using an Agilent 50 GHz vector network analyzer (VNA) N5225A and an Agilent 50 GHz lightwave component analyzer (LCA) N4373C to characterize the high-speed performance of the Si-LPIN GePD. Typical S_{21} transmission parameters as a function of frequency, at 1550 nm and

1310 nm wavelength, using an received average optical power of −6 dBm and −5 dBm are shown in Fig. 5(a) and Fig. 5(b), respectively. The received average optical power is the average optical power reaching the photodiode. At −1 V, the device shows a 3-dB opto-electrical bandwidth of >50 GHz and 45 GHz at 1550 nm and 1310 nm, respectively. The opto-electrical bandwidth is further enhanced to over 50 GHz for both wavelengths as the bias voltage is increased to −2 V. The opto-electrical 3-dB bandwidth data extracted from the wafer-scale measurement S_{21} curves for both wavelengths are shown in Fig. 5(c). At 1550 nm wavelength, the wafer-scale 3-dB bandwidth is over 50 GHz at both −1 V and −2 V bias voltage. At 1310 nm, the wafer-scale 3-dB bandwidth is over 50 GHz at −2 V. At −1 V, the mean 3-dB bandwidth value is 44 GHz with a standard deviation of 2.2 GHz. The standard deviation of bandwidth for conditions where the bandwidth is beyond 50 GHz could not be measured due to the bandwidth limitation of the VNA/LCA.

The lower opto-electrical 3-dB bandwidth of the Si-LPIN GePD at 1310 nm can be attributed to the longer carrier transit time at this wavelength. This is because the photo-generated carrier density (in the first absorption length) in the device is much higher at 1310 nm than that at 1550 nm due to the much stronger germanium absorption coefficient at 1310 nm. The electric field is partly screened by the photo-generated carriers. Therefore, the photo-carriers experience a lower drift velocity and so a longer drift time at 1310 nm, leading to a lower bandwidth. This effect is especially pronounced at low bias voltage.

The photodiode capacitance of the Si-LPIN GePD was extracted by fitting the real/imaginary part of the S_{22} reflection parameters (measured at wafer scale) based on an equivalent circuit model shown in the inset of Fig. 5(d). In the circuit model, C_j is the capacitance of the reverse biased p-i-n junction, and R_s is the series resistance related to the p-i-n junction. C_{OX} and R_{Si} are related to the current path through the silicon substrate and the buried oxide (BOX). C_m represents the metal pad capacitance. The metal pad capacitance C_m is firstly extracted by fitting the S_{22} parameter of an OPEN reference structure. Afterwards, using this C_m value, the full S_{22} parameter of the Si-LPIN GePD is fitted to extract the value of other components in the equivalent circuit model. The extracted junction capacitance (C_j) data and series resistance (R_s) data of the Si-LPIN GePD are shown in Fig. 5(e) and Fig. 5(f). The mean junction capacitance value is 6.8 fF and 6.2 fF at −1 V and −2 V, respectively. The mean series resistance value is 103 Ω and 91 Ω at −1 V and −2 V, respectively. One example of the experimental and fitted real/imaginary part of the S_{22} parameters is shown in Fig. 5 (d).

The opto-electrical bandwidth of the Si-LPIN GePD was further characterized for individual devices using an Agilent 67 GHz VNA E8361A and an Agilent 67 GHz LCA N4373B at 1550 nm wavelength. The measured S_{21} curves using an average received optical power of −5.5 dBm are shown in Fig. 6(a). At −1 V, the device shows a 3-dB opto-electrical bandwidth of ~67 GHz, and the bandwidth is enhanced to beyond 67 GHz as the bias voltage is increased to −2 V and −3 V. The dip around 15 GHz and the fast roll off between 64~67 GHz appearing on the S_{21} curves are attributed to the calibration of the VNA together with RF cables and RF probe used in the experiment. The impact of the optical input power on the opto-electrical bandwidth of the Si-LPIN GePD was also characterized using an Erbium-doped Fiber Amplifier (EDFA) together with a Variable Optical Attenuator (VOA) to control the input optical power. The measured opto-electrical 3-dB bandwidth as a function of the input optical power is shown in Fig. 6(b). A drop in the bandwidth can be observed at higher optical input powers, which is attributed to a screening of the internal electrical field in the photodetector due to the photo-generated carriers. This effect is especially pronounced at low bias voltages. It can be seen that at a bias voltage larger than −1 V, there is almost no drop of 3-dB bandwidth under an input optical power smaller than 1.3mW.
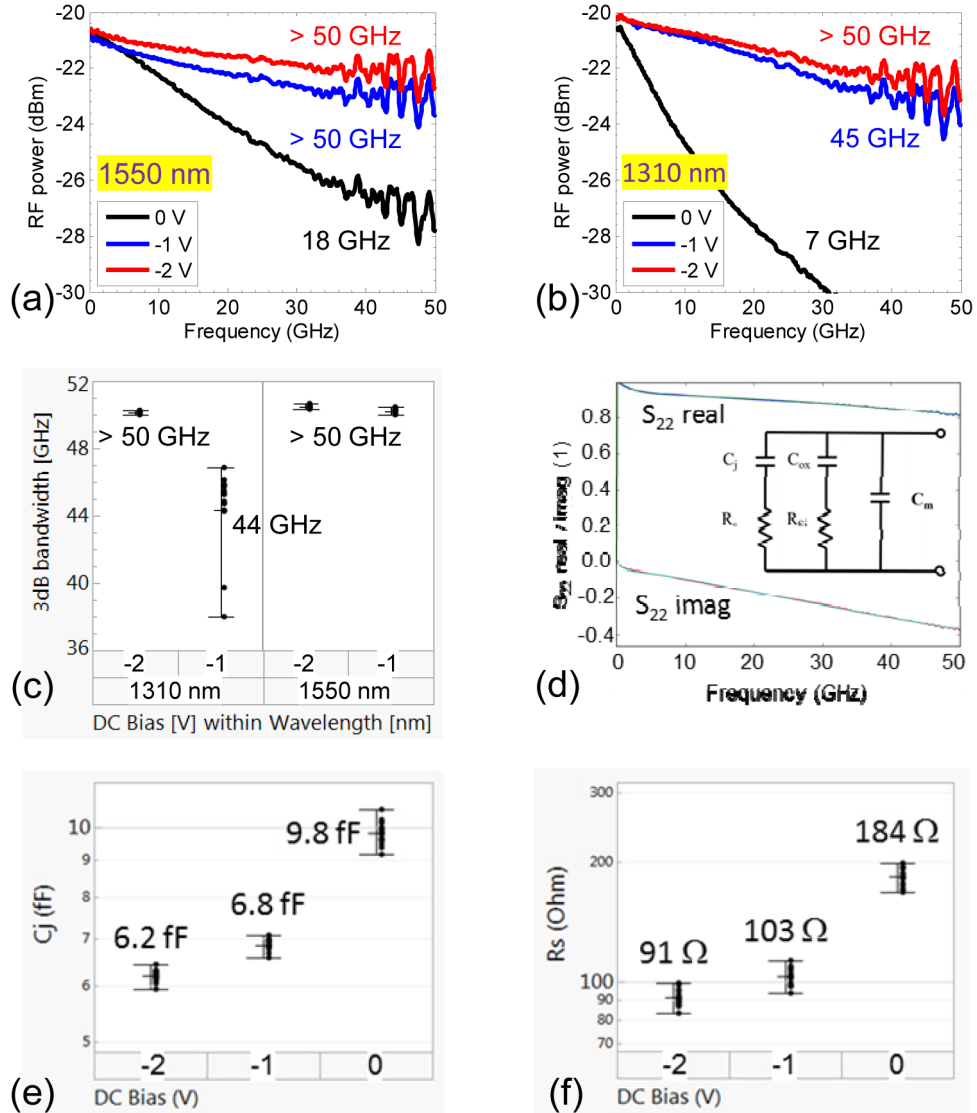
Fig. 5. Small-signal S21 transmission parameter as a function of frequency of the Si-LPIN GePD at (a) 1550 nm and (b) 1310 nm wavelength. (c) Variability plot of wafer-scale opto-electrical 3-dB bandwidth data. (d) Experimental and fitted real/imaginary part of the small-signal S_{22} reflection parameter. The inset is the equivalent circuit model used for the fitting. (e) Variability plot of the p-i-n junction capacitance data extracted from the fitting. (f) Variability plot of the series resistance data extracted from the fitting.
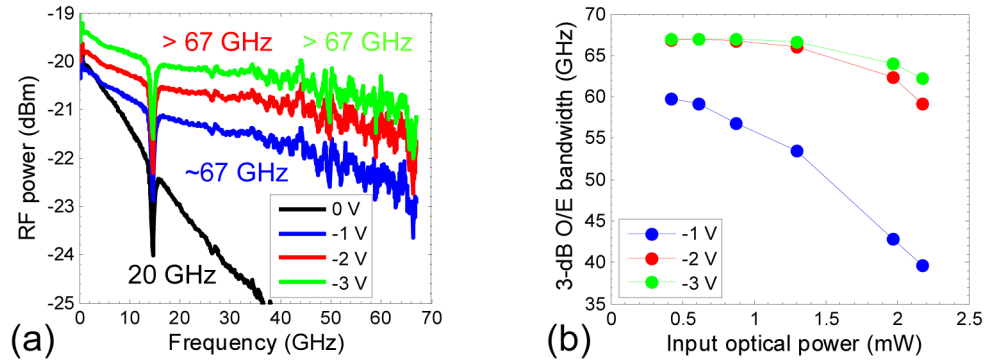
Fig. 6. (a) Small-signal S21 transmission parameter as a function of frequency of the Si-LPIN GePD at 1550 nm. (b) Measured 3-dB opto-electrical bandwidth as a function of input optical power at 1550 nm.

3.3 Large-signal measurements

On-off keying data reception experiments were implemented. A $(2^{31}-1)$ long optical non-return to zero (NRZ) pseudo random bit sequence (PRBS) data pattern at 50 Gbps and 56 Gbps, generated by a commercial LiNbO$_3$ modulator at 1550 nm was launched into the Si-LPIN GePD (56 Gbps is the upper limit of the pulse pattern generator operation range). A −1 V bias voltage was applied to the photodetector using a 50 GHz RF probe connected to a 40 GHz bias-tee. The output electrical data was measured with an Agilent infiniium sampling oscilloscope with a 60 GHz remote sampling head plug-in. The 50 Gbps and 56 Gbps reference transmitter eyes at 1550 nm wavelength are shown in Fig. 7(a)-7(b). The electrical eye diagrams from the Si-LPIN photodetector at −1 V are shown in Fig. 7(c)-7(d). The same experiment was also implemented at 1310 nm wavelength as shown in Fig. 8(a)-8(d). The clear open electrical eye diagrams from the Si-LPIN GePD at −1 V indicate the high quality data reception performance of the Si-LPIN GePD at 56 Gbps, in both the C-band and O-band.

4. Discussion and outlook

The frequency response of the equivalent circuit in Fig. 5(d) exhibits a 3-dB bandwidth of 120 GHz and 140 GHz at −1 V and −2 V assuming a 50 Ω load. Comparing these values to the experimental data reveals that the opto-electrical bandwidth of the Si-LPIN GePD is limited by the carrier transit time instead of the RC-constant. It can be seen from Fig. 2(a) that the photo-carriers will drift along the electric field in a non-linear trajectory before being collected. Moreover, certain photo-carriers will hit the top surface and/or the sidewall of the germanium layer in the drifting. This will increase the transit time compared to the simple case where photo-carriers drift in a straight line.

It can be seen from Fig. 2 that the thicker the germanium layer, the longer the carrier transit time in the Si-LPIN GePD device will be, and thus the lower the opto-electrical bandwidth. This is clear from Fig. 9(a), comparing the experimental S$_{21}$ curves for a germanium layer thickness of 160 nm and 400 nm (with the same the same germanium width of 500 nm). On the other hand, the modal absorption coefficient is larger for a device with a thicker germanium layer due to the larger modal confinement factor in the germanium layer. Therefore, the Si-LPIN GePD with a 400 nm thick germanium layer has a higher responsivity than that of the device with a 160 nm thick germanium layer (14.2 μm long), as shown in Fig. 9(b). Figure 9 indicates that the germanium layer thickness can be designed to optimize the opto-electrical bandwidth or responsivity performance of a Si-LPIN GePD device.
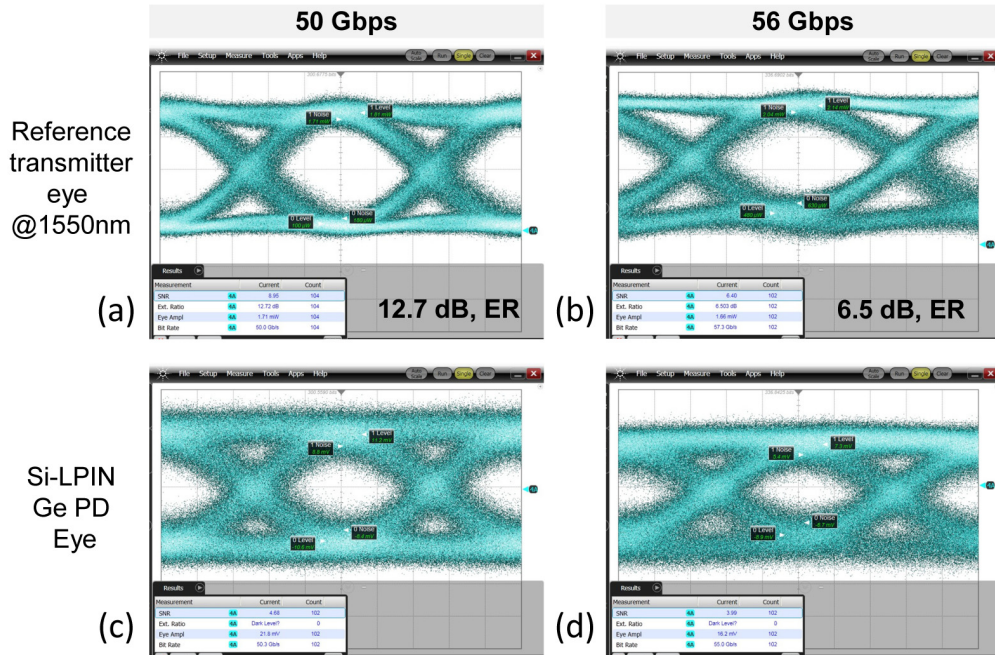
Fig. 7. The optical eye generated from a 1550 nm commercial LiNbO₃ Mach-Zehnder modulator at (a) 50 Gb/s and (b) 56 Gb/s. The corresponding electrical eye from the Si-LPIN GePD at −1 V bias at (c) 50 Gb/s and (d) 56 Gb/s.
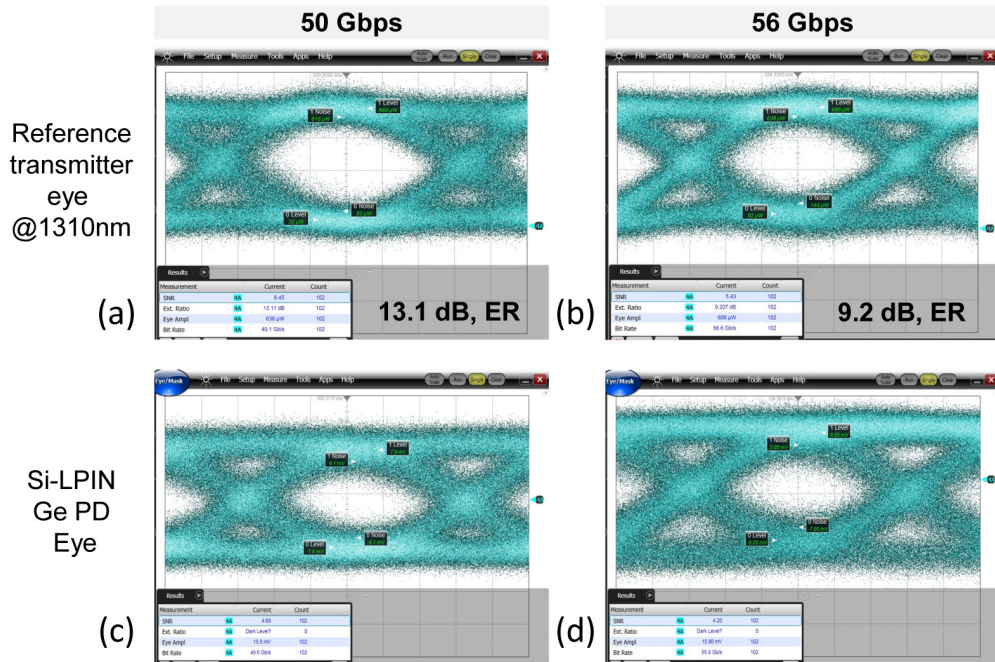
Fig. 8. The optical eye generated from a 1310 nm commercial LiNbO₃ Mach-Zehnder modulator at (a) 50 Gb/s and (b) 56 Gb/s. The corresponding electrical eye from the Si-LPIN GePD at −1 V bias at (c) 50 Gb/s and (d) 56 Gb/s.

The increased overlap of the optical mode with the doped silicon layers in the thin Ge device cannot account for the reduced responsivity at 1550 nm. Light absorption from the doped Si regions was quantified through optical simulation. At 1310 nm, the confinement factor of the fundamental optical mode in the Ge-on-SOI waveguide is 0.79 and 0.076 in the germanium layer and the doped Si layer (both N-doped region and P-doped region), respectively. Assuming a germanium material absorption coefficient of 7000 cm^{-1} and a N/P-doped Si absorption coefficient of 18 cm^{-1}/60 cm^{-1} [17], the modal absorption coefficient related to germanium absorption and doped Si absorption is 5538 cm^{-1} and 3.0 cm^{-1}, respectively. The same exercise is done at 1550 nm, and the (fundamental mode) modal absorption coefficient related to germanium absorption and the doped Si absorption is 1025 cm^{-1} and 7.5 cm^{-1}, respectively. The share of doped Si absorption in the total modal absorption coefficient is 0.05% and 0.73% at 1310 nm and 1550 nm, respectively. Although the doped Si absorption contributes more at 1550 nm than that at 1310 nm in the total modal absorption, its low absolute contribution (0.72% at 1550 nm) cannot explain the responsivity drop at long wavelength. Therefore, since the opto-electrical bandwidth is limited by the carrier transit time, the responsivity of the 160 nm thick Si-LPIN GePD at 1550 nm can be improved by increasing the length of the device without compromising on the opto-electrical bandwidth.
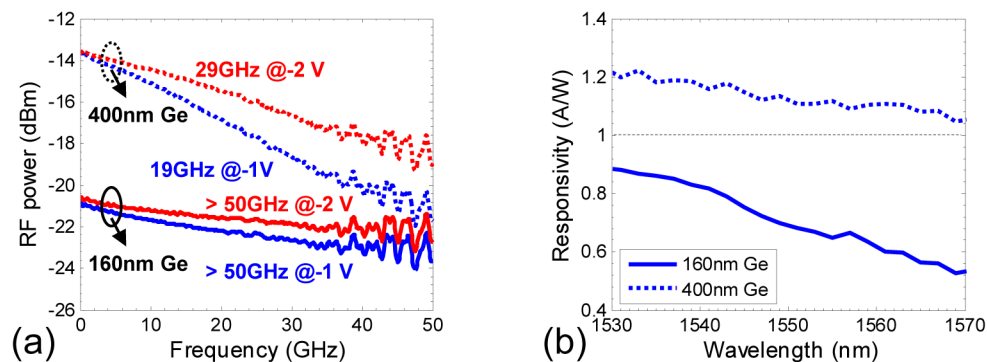
Fig. 9. (a) Small-signal S21 transmission parameters as a function of frequency at 1550 nm of the Si-LPIN GePD with a 400 nm thick Ge layer and a 160 nm thick Ge layer. (b) Responsivity as a function of wavelength in the C-band of the Si-LPIN GePD with a 400 nm thick Ge layer and a 160 nm thick Ge layer. The only difference between the 2 Si-LPIN GePD devices is the germanium layer thickness.

5. Conclusion

A 67 GHz germanium waveguide p-i-n photodetector that has neither doping in nor metal contacts on germanium operating at −1 V is reported. The device was characterized in both the C-band and O-band, showing low dark current and high responsivity. 56 Gbps on-off keying data reception is demonstrated. The opto-electrical 3-dB bandwidth beyond 67 GHz at higher reverse bias should enable even 100 Gbps on-off keying optical receivers.

Acknowledgments